Journal of Earth & Statistics

Journal homepage: http://www.Jes.arakut.ac.ir

Doi: 10.22034/jes.2022.556898.1008

Ministry of Science, Research & Technology
Arak University of Technology

Earthquake Hazard Zoning in Borujerd County with an Emphasis on Urban Development

***Ali Solgi*[1], *Ali Ghias Yeganeh*[2], *Ali Uromeie*[3], *Zahra Maleki*[1], *Nima Nezafati*[1]**

[1]Department of earth scicnces, scicnces and research branch, Islamic azad university,Tehran,Iran

[2] Director of Civil Engineering, Yasin Broujerd University

[3] Department of engeering geology tarbiat modares university,Tehran,iran

Article Info

Keywords:
Earthquake, Seismic Power, Probabilistic Approach, eterministic Approach

*Corresponding Author's Email Address: a.solgi@srbiau.ac.ir

Abstract

In this study, the study region is Zagros orogenic belt in the southwest of Iran and it is situated in the structural zones called Sanandaj-Sirjan (the northeastern half of the region) and crushed Zagros (southwestern half of the region). In this study, the basic Guttenberg-Richter method as well as the updated Kiko-Selovel method have been used and the Kiko-Selovel method is based on the double bounded Guttenberg-Richter distribution function so that the importance of applying novel methods can be more clarified through the comparison of the results. In order to investigate the depth phase of the earthquakes in the studied domain, the data obtained from the earthquakes' epicentral mechanism was utilized. To do so, the focal data of the studied region's design level earthquake mechanisms were extracted within a 200-kilometer distance from such credible websites as USGS, NEIC, and CMT and the form of their epicentral mechanism was drawn using WInTensor Software and based on the obtained results, the maximum seismic power of the intended faults ranges from 5.8 to 7.8 in the Richter scale. Moreover, the highest seismic powers were found respectively pertaining to Main Zagros's thrust fault (M=7.8), high Zagros (M=7.6), Kushk Nosrat (M=7.5), Lahbari 9M=7.5), F3 (M=7.4), Zardkuh (M=7.2) and Ardal (M=7.4). The largest horizontal accelerations obtained in the deterministic approach are 0.23g, 0.18g, and 0.17g, respectively. Furthermore, the largest horizontal and orthogonal accelerations in the probabilistic approach and the DBE design level are 0.30g and 0.14g,

Introduction

Earthquake is one of the natural phenomena on the planet earth and due to the lack of sufficient knowledge about it, it can be called a stochastic phenomenon. Considering the advancements in seismology, earthquake engineering and geology, appropriate scientific solutions have not been expressed for this phenomenon in spite of a great many of the discussions and researchers made in this regard. Since the only way for fighting this phenomenon is presently strengthening of the structures and relative reduction of the life losses as a result of the earthquakes, the reliable estimation and investigation of the earthquake hazard are deemed as inevitable necessities accordingly. In the reliable estimation of the earthquake hazard, all of the parameters that can influence the intended domain can be investigated and taken into account in the calculations. It can be generally stated that seismotectonic studies should be carried out in the region. In the seismotectonic studies, the relationships between the tectonic processes and the earthquakes occurrence are investigated as the first step in estimating earthquake hazard. In earthquake hazard analysis, it is quite likely that the amounts of the ground motion parameters be increased as a result of the earthquake occurrence in the potential sources within a specific period. In order to purposively describe and quantitatively estimate the earthquake hazard and evaluate the contingent effects in a construction site, it is necessary to perform an estimation of the ground motion within a certain distance from the earthquake occurrence locus. These estimations are usually obtained using equations known as attenuation relations that express the ground motion as a function of the earthquake magnitude and distance to the construction site as well as the conditions of the construction site. In this regard, researches have been carried out. Pakzad and Mirza'ei (2008) investigated the epicentral mechanism of the earthquake on 31st of March, 2006, in Darb-e-Astaneh, in Silakhor, using the linear transformation of torque's tensor within the area of time, primary earthquake mechanism and several foreshocks and aftershocks(Pakzad and Mirza'ei 2008). Teymuri (2008) has dealt in a research paper with the seismological attitudes of Tehran University and analyzed the earthquake on the 31st of March, 2006, in Silakhor (Teymuri 2008). Zamani and Agh-Atabai (2009) investigated the multifractal seismicity of Iran and expressed that almost all the Zagros earthquakes have occurred in the upper crust with an approximate depth of 15±7 kilometers with their magnitudes rarely reaching MW=7 (Zamani and Agh-Atabai 2008). Zibandehpour (2015) dealt in their research in geophysics with the earthquake hazard analysis and preparation of a uniform hazard spectrum for the city of Borujerd and expressed that the highest and lowest acceleration rates are seen in the western and eastern sides of Borujerd, respectively (Zibandehpour 2015). In a research on the seismology topics, Sepahvand (2011) investigated the seismotectonic features of the present era Zagros's primary fault in the distance between Dorud and Borujerd and stated that the aftershocks occur in depths ranging from 4km to 11km in this region and that they are shallower in contrast to the other spots on Zagros (Sepahvand 2011). Furthermore, the aftershocks' distribution is expressive of the existence of old faults in the northeastern wing of Silakhor plain to which no seismic activity has been attributed so far. Mauro Caccavale et al. (2017) offered and investigated an integrated approach for hazard zoning of the landslides stemming from earthquake based on probabilistic seismic hazard analysis (PSHA) scenario for Felger, Ishia, Prochida and Vivara Islands in Italy (Caccavale et al. 2017). In the end, the risk analysis of the landslides stemming from the earthquake was presented for the source region based on blending of the probabilistic approach and geological, morphological and geotechnical databases existent for the study region. The probabilistic seismic hazard analysis (PSHA) was carried out for defining the earthquake inputs featuring frequencies higher than annual values. Finally, based on the estimations of the annual landslides induced by earthquakes for every ground cell, a scale 1:5000 map was prepared for the risk of the landslides stemming from the earthquake for the aforementioned islands.

In research called zoning the risks stemming from an earthquake, Andrea Valagussa et al .(2014) offered a method for probabilistic quantitative earthquake hazard zoning in Frilui region (eastern Italy Alpine) regarding the 6.8MW earthquake in 1976 (Valagussa et al. 2014). Four sets of heavy data were prepared following the historical data analysis and field investigation. This methodology relies on a 3D hazard vector comprised of heavy dynamic energy, flight height, and annual frequency. The amounts of the first two indicators were calculated for every place along the slope using the simulator Software Runout 3D Rockfall Hy-STONE. The annual precipitation frequency is evaluated through multiplying the annual initial frequency by the simulated transit frequency. The annual onset frequency is computed based on a method composed of the extents of the unstable regions for ten various seismological scenarios with various annual occurrence frequencies and the relative frequency-blocks relationship based on the collected field data. For every annual occurrence frequency, the unstable region is calculated as a function of the morphometric properties and earthquake. The results indicated that the slope curvature plays an important role in the calculation of the unstable zone.

Based on the studies conducted by Ruchi Singh (2019) regarding the earthquake faults zoning and values of the real estates in 1972, the Alquist-Priolo zoning rule enabled the publication of earthquake fault maps for California (Singh 2019). Based thereon, these formal maps were gradually revised over time for estimating the investment rate concering the seismic hazard of the valuated real estates. Using the consistent geographical data collected from 1970 to 2010 in a census, it was observed that the value of the real estate has undergone reductions by 6.6% after the specification of a fault zone therein whereas the rentals were only found reduced by about 3.3%. In addition, the analysis of the micro-scale transaction data from 1997 to 2016 is suggestive of the idea that the prices of the houses have been increased by 1.8% in the regions one mile away from the fault zone.

Mohsen Kuhrangi et al. (2018) dealt in a study with the comparison of the results obtained for the hazard model of the earthquake that occurred in 2014 in the Middle East (EMME14) and the national seismic designing codes in Iran (Kohrangi et al. 2018). According to them, the regional seismic hazard models of several countries can be used as a basis of comparison with the national seismic hazard models that are generally used for supporting the national construction codes regarding the design level seismicity. In this study, as an example, the seismic design spectrum of Iran's national design code was compared with the uniform hazard spectrum of the recent earthquake hazard for the Middle East Region (EMME) in a completely coordinated manner. This comparison is concentrated in two maps of 10% likelihood of transcending beyond 50 years for PGA and pairs of design spectrums for four cities with various seismographic levels. While the two reference PGA maps seem to be similar in rock, the comparison of the uniform hazard spectrum and the design spectrums for the four selected cities show large differences in various soil conditions. Ismailzadeh et al. (2018) dealt in a study with the quantitative modeling of lithosphere dynamics, earthquakes and seismic hazard (Ismail-Zadeh et al. 2018). Based on their studies, modeling the lithosphere's dynamicity and simulation of an earthquake along with the seismic hazard analysis can offer better evaluations of the potential earth vibrations stemming from an earthquake. Based thereupon, in this study, a dynamic block fault model (BAFD) was offered that simulates the earthquake based on the lithosphere's dynamicity and enables the investigation of the effect of fault network's properties and regional motions according to the seismological patterns. Song et al. (2018) evaluated the contingent risk of landslide stemming from an earthquake in a study (Song et al. 2018). According to the fact that the earthquake-induced ground motions can differ in various horizontal directions, these directing changes should be embedded in the evaluation of earthquake-induced landslide risk. Thus, the study investigated the effect of ground motions' direction on the probabilistic seismic displacement hazard in the slopes.

Artikov et al. (2016) studied the accuracy and precision of the modern seismic zoning maps in the eastern section of Uzbekistan in a study (Artikov et al. 2016). In line with this, the effect of the input parameters' uncertainty on the seismic hazard estimation results was explored. The results indicated that the highest deviations from the seismic hazard maps designed based on the mean values of the seismic state distribution and seismic load parameters may provide uncertain estimations of the seismic potential (Mmax) and recurrence curve's slope (γ) due to the incorrect depth of the seismic sources (H) with the share of such factors as incorrect definition of seismic activity (A10) and incorrect selection of the dominant motion type in the source using the regional regulations being trivial due to the reductions in the seismic load's intensity in distant places instead of exact values once for every locality.

Pradhan et al. (2010), as well, used a back-propagative neutral network based on GIS in a study to perform landslide hazard zoning in Malaysia (Pradhan and Lee 2010). Kavazoglou et al .(2015) suggested a solution for selecting the most appropriate factors influencing the landslide using the genetic algorithm and showed the way to achieve an optimal combination of factors from amongst the numerous factors via investigating the general precision of each of the subsets (Kavzoglu et al. 2015).

The study region in the present study is located in the northwestern extent of the tectonic Zagros and Sanandaj-Sirjan zone in latitude between 33.60 and 34.12 and longitude between 48.46 and 49.08 within the realm of Borujerd County. Due to the absence of sufficient information and data, it is not possible to express the attenuation relations suitable for the intended region so the attenuation relations calculated at the global level are utilized.

Study Method

In the present study, a catalog was seminally prepared for the historical natural and machinery-induced earthquakes that had occurred in the region in order to perform seismic analysis thereof. Then, according to the existent resources (reports, credible scientific articles, seismotectonic maps and so on), the active faults and seismic sources of the region were determined following which the region's seismotectonic map was delineated. In the end, use was made of the seismic data and seismic faults to analyze the region's seismicity and offer the seismic zoning map of the region. The earthquake hazard analysis includes such a primary stage as gathering seismic data. Table 1 gives the most important historical earthquakes that have occurred in the region: the investigation of the data reliability and filtering of the non-seismic data, magnitude analysis, estimation of the maximum magnitude, analysis of the depths of the earthquakes' epicenter, estimation of the seismological parameters, determination of the seismic sources, estimation of the seismic sources' parameters, selection of attenuation relations, estimation of the maximum values of the credible ground motion parameters based on deterministic method and final estimation of the ground motion parameters for the various designing stages.

Table 1. Specifications of the historical earthquakes in the studied extent

No.	Date	Time	X	Y	Ms	Ref.
1	c.1.8 Ma		50.78	36.11	7	BER
2	c.11000 BP		47.6	33	7	BER
3	c.4000-3350 BP		47.92	34.45		BER
5	224-642		47.93	34.45		BER
6	872/06/21		47.15	33.11		BER
7	872/06/22		47.2	33.2	6.8	AMB
8	956		48.1	34.8	5.3	AMB
9	987/11		48.5	34.8	5.9	ULM
10	1008/04/27	18	47.4	34.6	7	AMB
11	1087/11		48.5	34.8	5.9	AMB
12	1107/09		47.4	34.6	6.5	AMB
13	1119/12/10	18	49.9	35.7	6.5	AMB
14	1177/05		50.7	35.7	7.2	AMB
15	1191		48.5	34.8		AMB
16	1316/01/05		49.4	33.5	6.2	AMB
17	1430		48	34.5	5.9	AMB
18	1495		50	34.5	5.9	AMB
19	1666		50.5	32.1	6.5	AMB
20	1721/07		50.2	35.68		BER
21	1853/06/11		50.3	32.6	5.5	AMB
22	1872/06		47.7	34.7	6.1	AMB
23	1876/09/28	3	49.7	33.1	5.8	AMB
24	1876/10/20	15	49.8	35.8	5.7	AMB
25	1880		50.65	32.02	5.3	BER

The published information and catalogs including the data offered by Nowruzi (1976) and Berberian (1977), ISC's catalog of the earthquakes, the earthquake catalog of Europe-Mediterranean Sea and the catalog published by Genes and Nelson (1981), were also used case-specifically (Nowroozi 1976; Berberian and Navai 1977). In this study, Guttenberg-Richter Base Method, as well as the updated Kiki-Seluvel Method which is based on the double bounded Guttenberg-Richter distribution function, were also employed for comparing the earthquakes' frequency and magnitude so that the importance of applying novel methods can be more highlighted. The results obtained from the statistical investigations of the earthquakes' epicenters within the study region are reflective of the considerable increase in the number of earthquakes with epicenters in depths ranging from 8km to 12km (about 48% of the entire data). Table 2 gives the faults introduced as the region's seismic sources through blending of the information obtained in the prior research including the map of Iran's active faults (Hesamiazar et al, 2003) and the seismic data as well as the epicentral mechanism of the earthquakes occurred within the study breadth.

Journal of Earth & Statistics
Journal homepage: http://www.Jes.arakut.ac.ir
Doi: 10.22034/jes.2022.556898.1008
Ministry of Science, Research & Technology
Arak University of Technology

Table 2. Seismic sources within a 200-kilometer radius from the city of Borujerd

Row	Fault name	Mechanism	Fault length (km)	Row	Fault name	Mechanism	Fault length (km)
1	South of Parandak	Reverse	10.73	12	Morvarid	Strike-slip	136
2	Kushk Nosrat	Reverse	222.5	13	F3	Reverse	172
3	F1	Reverse	110	14	H.Z.F	Reverse	360
4	Indes	Reverse	97	15	Zard Kuh	Reverse	141
5	F2	Reverse	58	16	Ardal	Reverse	175
6	Tafresh	Reverse	118	17	M.F.F.1	Reverse	43.3
7	M.Z.R.F	Reverse	650	18	M.F.F.2	Reverse	15
8	Dorud	Strike-slip	104	19	M.F.F.3	Reverse	91.7
9	Nahavand	Strike-slip	104	20	Balarud	Reverse	175
10	Garon	Strike-slip	25	21	Lahbari	Reverse	235
11	Sahneh	Strike-slip	84				

To better compare the results, the earthquakes that occurred within a 200-kilometer radius from the center of Borujerd County have been examined following which statistical methods like least squares were used to calculate the coefficients (a-value and b-value) in Guttenberg-Richter base method. It is worth mentioning that the main earthquakes following the earthquake declustering have been utilized for calculating Guttenberg-Richter's base coefficients. In order to investigate the depth mechanism of the study region's earthquakes, the data obtained from the earthquakes' epicentral mechanism were applied. To do so, the focal action mechanism data of the earthquakes occurred within a 200-kilometer radius of the study region were extracted from such credible websites as USGS, NEIC, and GMT and their epicentral mechanism forms were drawn using WinTensor Software.

Study Region

Borujerd is a county in the west of Iran. It is situated in the northern section of Lorestan Province. The county is positioned in Zagros's mountainous region with its center being the city of Borujerd. Borujerd County's limits are stretched to Malayer and Nahavand Counties in Hamadan Province in the north, to Shazand County in Markazi Province in the east, to Dorud County in the south and Khorram Abad and Selseleh Counties in the west.

The highest point of Borujerd County is Volash Apex, 3987m in height, in the west and the lowest region is on Silakhor Plain with an approximate height of 1500m. Borujerd County is part of northern Zagros's mountainous region which is comprised of elevated mountains of Zagros in the west and south, Silakhor Plain in the center and internal Zagros's foothills in the east and north. The elevated mountains of Zagros are stretched in a strap from the northwest to the southeast of the region and they are envisioned as the natural border between Silakhor Plain and the historical land of Lorestan. The large Garin or Garry Mountain Range with a length of 185km is part of the Elevated Zagros and it is stretched from the northwest to the southeast with Oshtorankouh following it as a tail. The most major apices of this mountain range are Chehel Nabaleqan and Volash, 3987m in height, and Mishparvar.

Borujerd County is located in the west of Iran in the northern section of Lorestan Province. The highest point in Borujerd County is the Volash Apex, 3978 meters in height, in the west of Borujerd County and the lowest region is in Silakhor Plain with an approximate elevation of 1500 meters. Borujerd County is part of the mountainous region in northern Zagros. The area of Ashtarinan and Borujerd Plains in the watershed basin of Silakhor River is over 1125 square kilometers. Silakhor Basin is bordered by Malayer Plain Watershed Basin in the north, by Marbarreh River Watershed Basin in the south, by internal Arak Watershed Basin in the east and northeast and by Harrud Watershed Basin and Chagholvandi Plain respectively in the west and southwest. In 2016, the population of Borujerd County has been 326452 individuals out of whom 163828 were male and 162624 were female.

The study region is a part of Zagros's orogenic belt in the southwest of Iran that is positioned in two structural zones of Sanandaj-Sirjan (northeastern half of the region) and crushed Zagros (southwestern half of the region). In terms of seismotectonic, the study area is spread over the northeastern half, central Iran and southwestern half of Zagros.

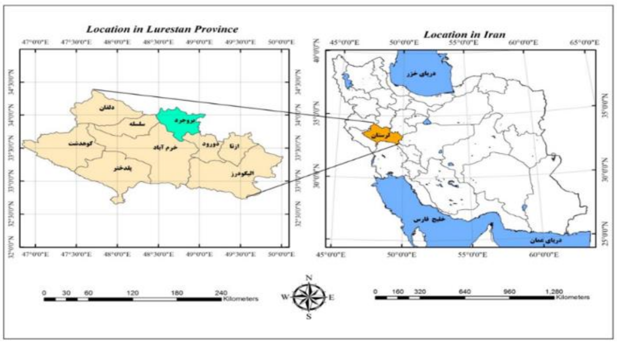

Fig. 1. The position of the study region in Iran (right-hand side) and Lorestan Province (left-hand side).

Results

A) Earthquake Hazard Analysis with the Study Region's Realm

To select the attenuation relation, a relationship must be used that is most consistent in terms of the seismotectonic with the studied region. To do so, attenuation relations by Zare'e (2004) have been used; amongst the accelerations, the largest has been chosen (Zare'e 2005). In general, in doing researches pertinent to earthquake hazard analysis in a given construction site, two essential approaches can be used. The first method is deterministic seismic hazard analysis (DSHA) and the second is the probabilistic seismic hazard analysis (PSHA).

B) Earthquake Hazard Analysis Using Deterministic Method

Stage One: Identification of Seismic Sources

This stage must investigate all of the seismic sources in the periphery of the intended construction site that can cause a devastating earthquake. The determination of the seismic sources is conducted based on the geological, geophysical and seismological data.

Stage Two: Selection of Controlling Earthquakes

After all the sources were determined, the controlling earthquakes should be specified for every seismic source. The specifications of the controlling earthquakes largely depend on the structure or construction site to be studied regarding the idea as to what dangers and risks can destroy it. For a structure, demolition of which is possible with low risk, the controlling earthquake can be considered as an incident that the occurrence likelihood of which is somewhat high during the useful life of the structure.

Zare'e (1999) has offered the following relation for calculating the fault disintegration length (on the earth surface) based on the exponential correlation between the disintegration lengths of 22 seismic faults in Iran (Zare'e 2005):

$$MW = 0.9\ \mathrm{Ln}(LR) + 3.66 \qquad (1)$$

Where LR is the surface rupture length as a result of the seismic fault's movement (in kilometers)

$$LR = 0.37 \times LF \qquad (2)$$

Ambraseys relation is also in the form shown beneath:

$$Ms = 4.629 + 1.429\mathrm{Log}(LR) \qquad (3)$$

Table 3. Maximum seismic power using experimental relations

Fault name	Mechanism	Fault length (km)	Rupture length (km)	Amberseys	Coopersmith	Zare'e	Mean
South of Parandak	Reverse	107.3	53.65	7.1	7.1	7.0	7.1
Kushk Nosrat	Reverse	222.5	100	7.4	7.4	7.6	7.5
F1	Reverse	110	55	7.1	7.1	7.0	7.1
Indes	Reverse	97	48.5	7.0	7.0	6.9	7.0
F2	Reverse	58	29	6.8	6.8	6.4	6.7
Tafresh	Reverse	118	59	7.1	7.1	7.1	7.1
M.Z.R.F	Reverse	650	100	7.4	7.4	8.6	7.8
Dorud	Strike-slip	104	52	7.1	7.1	6.9	7.0
Nahavand	Strike-slip	104	52	7.1	7.1	6.9	7.0
Garon	Strike-slip	25	12.5	6.4	6.4	5.7	6.1
Sahneh	Strike-slip	84	42	7.0	7.0	6.8	6.9
Morvarid	Strike-slip	136	68	7.2	7.2	7.2	7.2
F3	Reverse	172	86	7.3	7.3	7.4	7.4
H.Z.F	Reverse	360	100	7.4	7.4	8.1	7.6
Zard Kuh	Reverse	141	70.5	7.2	7.2	7.2	7.2
Ardal	Reverse	175	87.5	7.3	7.3	7.4	7.4
M.F.F.1	Reverse	43.3	21.65	6.7	6.6	6.2	6.5
M.F.F.2	Reverse	15	7.5	6.1	6.1	5.2	5.8
M.F.F.3	Reverse	91.7	45.85	7.0	7.0	6.8	7.0
Balarud	Reverse	175	87.5	7.3	7.3	7.4	7.4
Lahbari	Reverse	235	100	7.4	7.4	7.7	7.5

As it is observed in the above table, the maximum seismic power of the intended faults is in a range from 5.8 to 7.8 on average on the Richter scale. In addition, the highest seismic power was found pertaining to the main Zagros thrust faults, high Zagros, Kushk Nosrat, Lahbari, F3, Zardkuh and Ardal.

Stage Three: Selecting the Proper Attenuation Relationship

The attenuation relationship offered by Zare'e is as shown below:

$$Log(PGA) = a_1 M + a_2 M^2 + b.Log(R) + c_i S_i + \sigma P \qquad (4)$$

To calculate PGA, use has been made of the coefficients presented in table 4.

Table 4. Acceleration attenuation coefficient in the attenuation relationship proposed by (Zare'e 2005)

PGA	a1	a2	b	c1	c2	c3	c4	s
Horizontal	0.5781	-0.0317	-0.4352	-2.6224	-2.5154	-2.4654	-2.6213	0.2768
Vertical	0.5593	-0.0258	-0.6119	-2.6261	-2.6667	-2.5633	-2.7346	0.2961

Stage Four: Calculation of Strong Ground Motion Parameters for Design Level Analysis

Using the attenuation relationships (stage three) for the controlling earthquakes pertinent to each seismic source, the maximum motion (acceleration) of the ground is calculated. In this state, the earthquake creating the highest PGA in the construction site is considered as the design level seismic motion. Based on the aforementioned calculations for the seismic power and the distance of the modeled faults from the center of the city of Borujerd and application of the proper attenuation relations, the maximum acceleration values have been computed for each of the main seismic sources in respect to the construction site. In this investigation, the high Zagros, Nahavand, and Dorud Faults were found creating the highest accelerations in the study region due to their closeness to the studied construction site as compared to the other faults (Tables 5 and 6).

Table 5. Values calculated for the maximum horizontal acceleration based on the deterministic approach

Linear seismic source's name	Magnitude	Distance to the construction site (km)	Zare'e	Largest PGA
South of Parandak	7.1	215	0.09	0.09
Kushk Nosrat	7.5	186	0.11	0.11
F1	7.1	163	0.11	0.11
Indes	7	175	0.10	0.10
F2	6.7	137	0.10	0.10
Tafresh	7.1	123	0.12	0.12
M.Z.R.F	7.8	230	0.11	0.11
Dorud	7	53	0.17	0.17
Nahavand	7	50	0.17	0.18
Garon	6.1	60	0.11	0.11
Sahneh	6.9	94	0.15	0.15
Morvarid	7.2	150	0.12	0.12
F3	7.4	205	0.10	0.10
H.Z.F	7.6	68	0.17	0.23
Zard Kuh	7.2	206	0.10	0.10
Ardal	7.4	220	0.10	0.10
M.F.F.1	6.5	190	0.08	0.08
M.F.F.2	5.8	168	0.06	0.06
M.F.F.3	7	157	0.10	0.10
Balarud	7.4	135	0.13	0.13
Lahbari	7.5	205	0.11	0.11

Table 6. Values calculated for the maximum orthogonal acceleration based on the deterministic approach

Linear seismic source's name	Magnitude	Distance to the construction site (km)
South of Parandak	7.1	215
Kushk Nosrat	7.5	186
F1	7.1	163
Indes	7	175
F2	6.7	137
Tafresh	7.1	123
M.Z.R.F	7.8	230
Dorud	7	53
Nahavand	7	50
Garon	6.1	60
Sahneh	6.9	94
Morvarid	7.2	150
F3	7.4	205
H.Z.F	7.6	68
Zard Kuh	7.2	206
Ardal	7.4	220
M.F.F.1	6.5	190
M.F.F.2	5.8	168
M.F.F.3	7	157
Balarud	7.4	135
Lahbari	7.5	205

C) Earthquake Hazard Analysis Using Probabilistic Approach:

Stage One: Identification of the Seismic Sources

Seismic sources and their specifications have been completely given in table 2.

Stage Two: the Relationship between the Magnitude Repetition and Determination of Recurrence Mean

The second step is the linear data estimation and determination of the Guttenberg-Richter relationship and specification of the magnitude probability density function and delineation of its curve.

$$\text{Ln } N = \alpha - \beta M \qquad (5)$$

In the majority of the methods of probabilistic hazard analysis methods, the lower limit of threshold size is in a range between 4 and 5 and because one maximum limit can be considered for the magnitude, the probability density function of the magnitude can be expressed as shown underneath:

$$f(M) = C_1.\beta_1.e^{-\beta_1(M-m_0)} \qquad (6)$$

$$C_1 = \frac{1}{1 - e^{-\beta_1(M-m_0)}} \qquad (7)$$

Resultantly, the earthquake occurrence likelihood in each part of the seismic source is equal in various distances (number of segments=1). For an earthquake incident, the probability of its magnitude being situated in the i-th section of the entire magnitudes is calculated as shown beneath:

$$P(M_i - \frac{\Delta M}{2} \le M \le M_i + \frac{\Delta M}{2}) = f(M_i).\Delta M \qquad (8)$$

Stage Three: Calculation of Ground Motion

When the seismic sources were recognized and the recurrence relationship was specified with m_{max} and m_0 values, it is necessary to select the appropriate attenuation relationship according to seismic sources' mechanism of action and geological conditions for the estimation of strong ground motions. Then, in order to use the ground motion values in the probabilistic earthquake hazard analysis, the magnitude values and the distances of them should be obtained.

Stage Four: Calculation of Hazard Curve for the Construction Site

The possibility of ground motion increased in the k-th seismic source of a chosen acceleration is obtained from the following figures: It has to be noted that the above relation shows the probability of the occurrence of an earthquake with a maximum acceleration larger than the intended acceleration hence the prospective earthquake occurrence likelihood is not demonstrated.

According to the above-presented descriptions, the magnitude probability density function for the introduced seismic sources within the study region's extent is as displayed beneath:

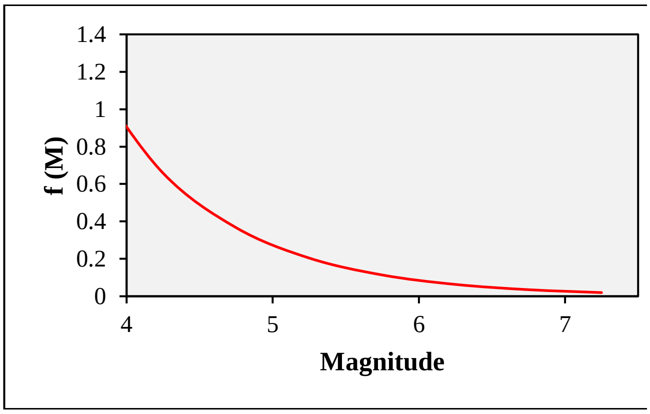

Fig 2. Magnitude probability distribution function for the seismic sources within the study region

Considering the distances equal to ΔM=0.5 for magnitude, the center of each distance (M_{mid}) is used. The likelihood in which the earthquake might occur with the obtained magnitude in the previous distances is as shown in Fig 3.

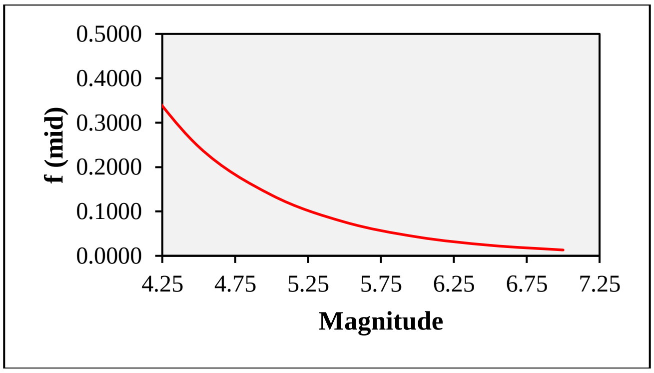

Fig 3. Earthquake occurrence likelihood within the various distances for the seismic sources in the study region

According to the abovementioned materials, the earthquake hazard analysis was conducted based on the probabilistic approach for some of the primary introduced seismic sources that will be dealt with in separate.

D) Seismic Source One: Southern Parandak Fault

A) Determination of Maximum Horizontal Acceleration

PGA values for the different magnitudes and distances of each section of seismic source 1 to the center of Borujerd are as shown in Fig 4 and 5.

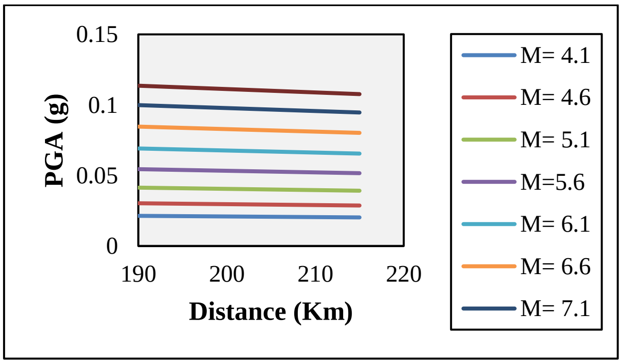

Fig 4. Attenuation estimation for Southern Parandak Fault (Zare'e-Horizontal Component)

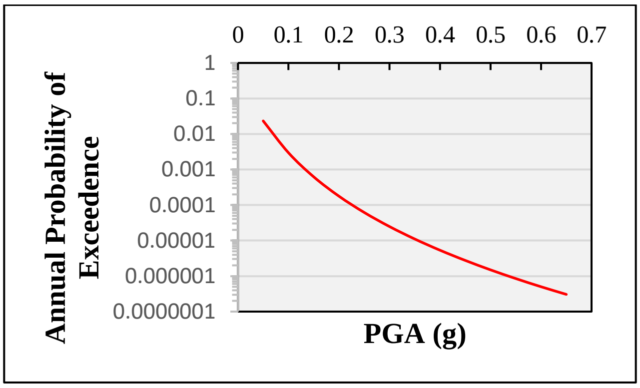

Fig 5. earthquake hazard curve for Southern Parandak Fault (Zare'e-Horizontal Component)

Determination of the Maximum Orthogonal Acceleration:

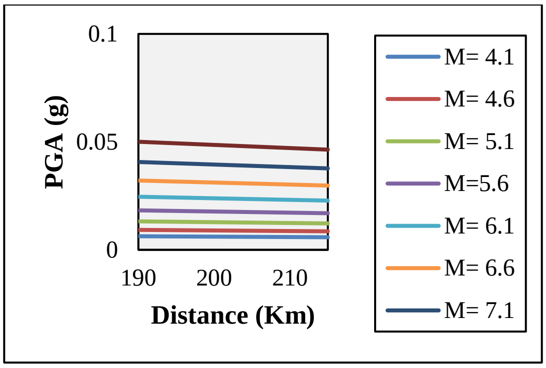

Fig 6. Attenuation estimation for Southern Parandak Fault (Zare'e-Orthogonal Component)

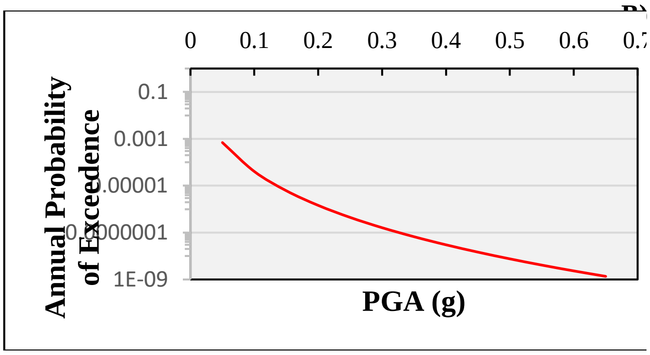

Fig 7. earthquake hazard curve for Southern Parandak Fault (Zare'e-Orthogonal Component)

Seismic Source Two: Kushk Nosrat Fault

A) Determination of the Maximum Horizontal Acceleration:

PGA values per the magnitudes and different distances of each segment from Kushk Nosrat Fault (seismic source 2) to the center of Borujerd are as shown in Fig 8 and 9.

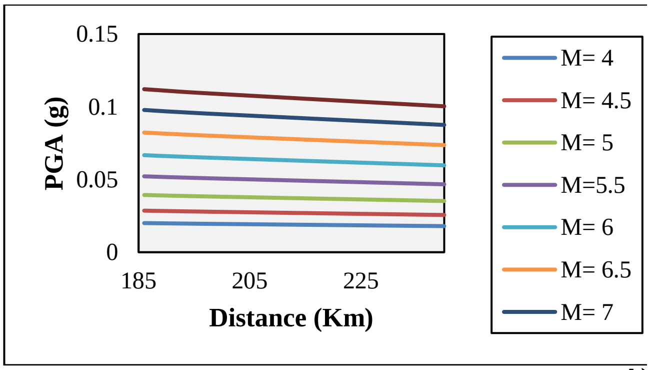

Fig 8. Attenuation estimation for Kushk Nosrat Fault (Zare'e-Horizontal Component)

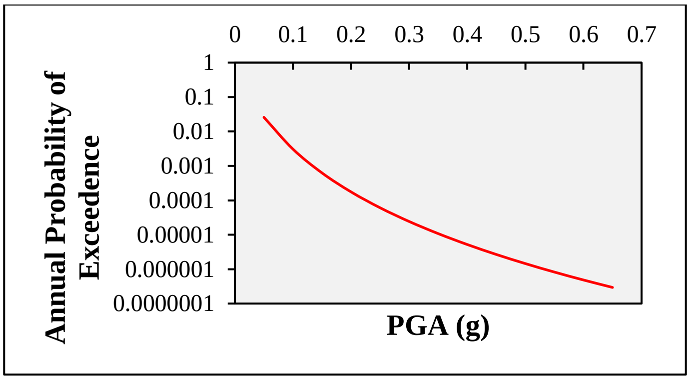

Fig 9. Earthquake hazard curve for Kushk Nosrat Fault (Zare'e-Horizontal Component)

B) Determination of Maximum Orthogonal Acceleration:

Fig 10 and 11 demonstrate the attenuation estimations of the orthogonal acceleration component according to the relations offered by Zare'e.

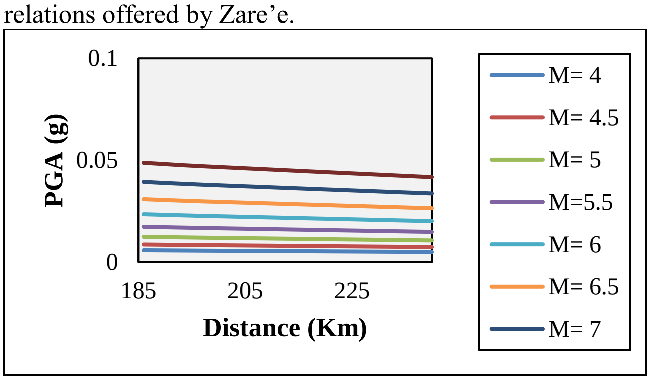

Fig 10. Attenuation estimations for Kushk Nosrat Fault (Zare'e-orthogonal component)

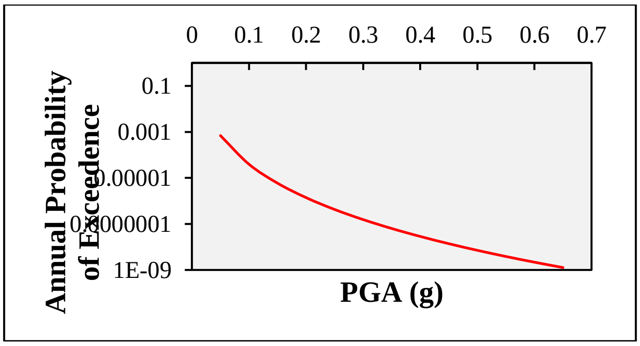

Fig 11. Earthquake hazard curve for Kushk Nosrat Fault (Zare'e-orthogonal component)

Seismic Source Three: F1 Fault

A) Determination of the Maximum Horizontal Acceleration:

PGA values per magnitude and different distances of each segment from F1 Fault (seismic source 3) to the center of Borujerd are as shown in Fig 12 and 13.

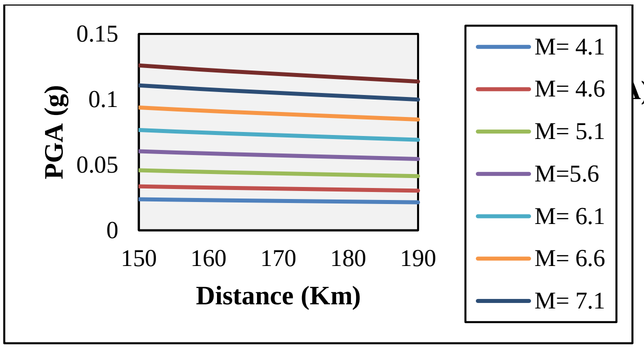

Fig 12. Attenuation estimation for F1 Fault (Zare'e-Horizontal Component).

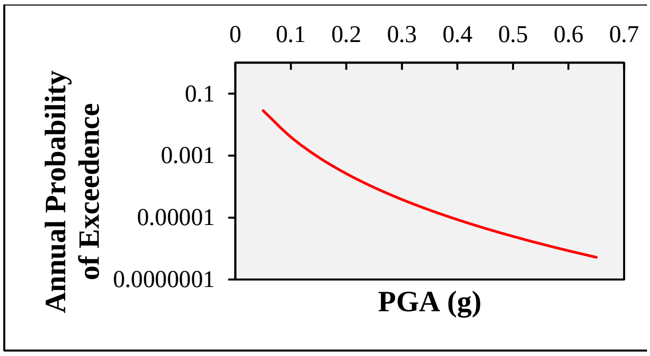

Fig 13. Earthquake hazard curve for F1 Fault (Zare'e-Horizontal Component)

B) Determination of Maximum Orthogonal Acceleration:

Fig 14 and 15 illustrate the attenuation estimation for the orthogonal acceleration component according to the relations offered by Zare'e.

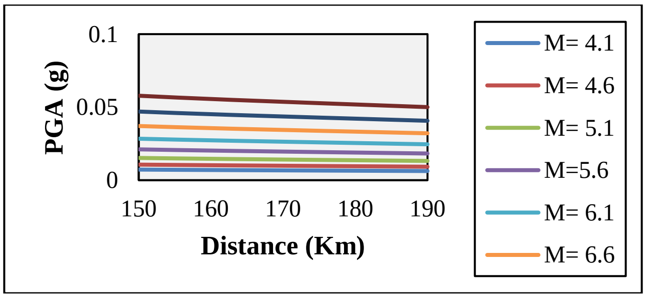

Fig 14. Attenuation estimation for F1 Fault (Zare'e-Orthogonal Component).

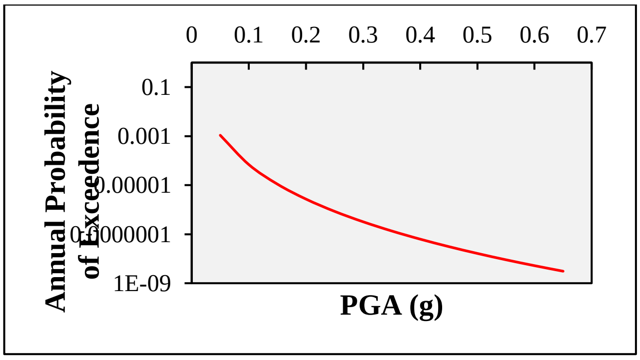

Fig 15. Earthquake hazard curve for F1 Fault (Zare'e-Orthogonal Component)

Seismic Source Four: Indes Fault

A) Determination of Maximum Horizontal Acceleration:

PGA values per magnitudes and different distances of each section of Indes Fault (seismic source 4) to Borujerd City's center are as displayed in Fig 16 and 17.

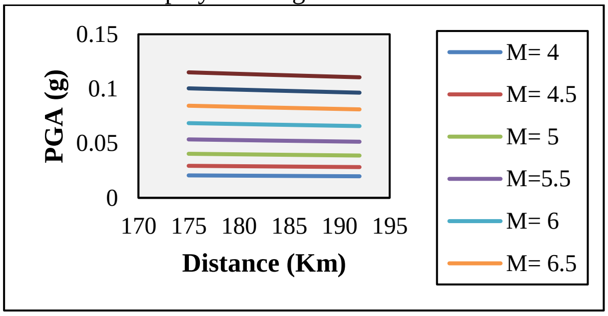

Fig 16. Attenuation estimation for Indes Fault (Zare'e-Horizontal Component).

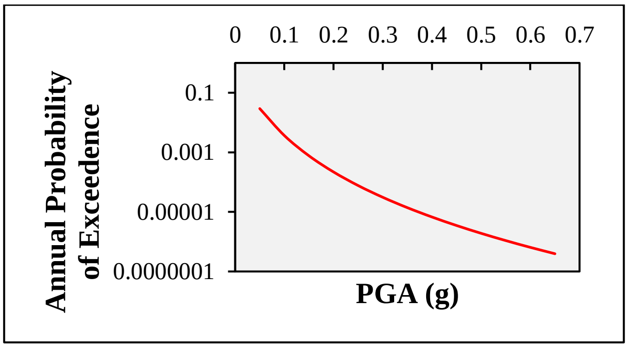

Fig 17. Earthquake hazard curve for Indes Fault (Zare'e-Horizontal Component)

B) Determination of the Maximum Orthogonal Acceleration:

Fig 18 and 19 depict the attenuation estimations of the orthogonal acceleration component according to relations presented by Zare'e.

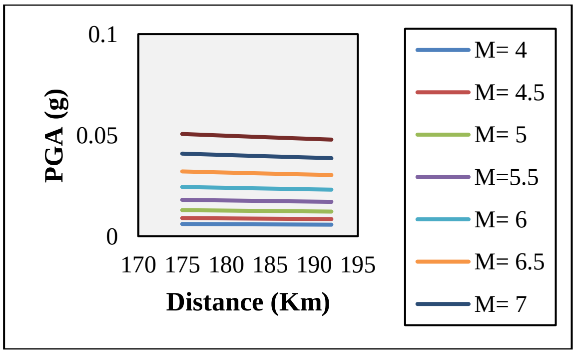

Fig 18. Attenuation estimation for Indes Fault (Zare'e-Orthogonal Component)

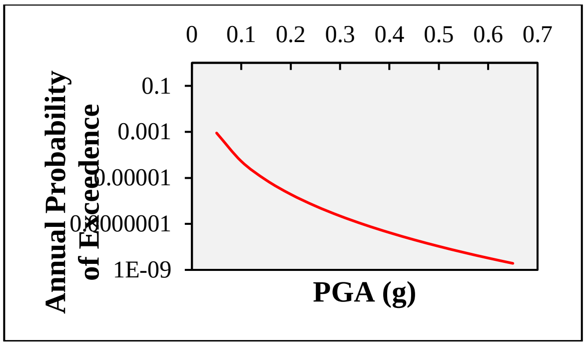

Fig 19. Earthquake hazard curve for Indes Fault (Zare'e-Orthogonal Component)

Seismic Source Five: F2 Fault

A) Determination of Maximum Horizontal Acceleration:
PGA values per the different magnitudes and distances of each part of F2 Fault (seismic source 5) from the center of Borujerd are as shown in Fig 20 and 21.

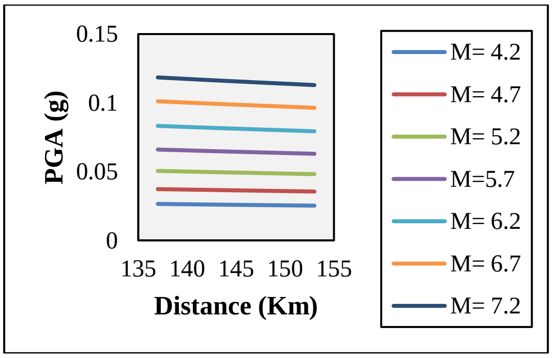

Fig 20. Attenuation estimations for F2 Fault (Zare'e-horizontal component)

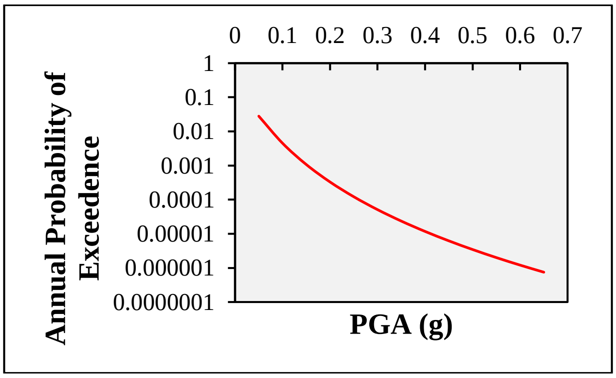

Fig 21. Earthquake hazard curve for F2 Fault (Zare'e-horizontal component)

B) Determination of the Maximum Orthogonal Acceleration:
Fig 22 and 23 portray the attenuation estimations of the orthogonal acceleration component according to the relations proposed by Zare'e.

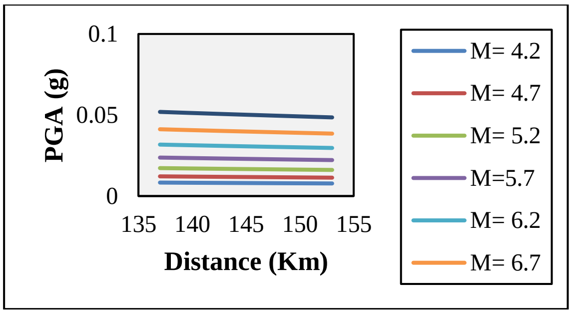

Fig 22. Attenuation estimation for F2 Fault (Zare'e-orthogonal component)

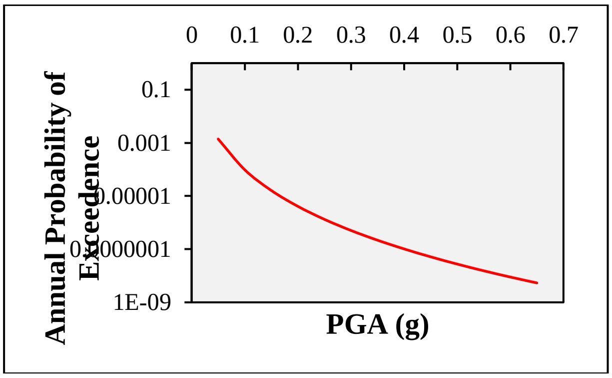

Fig 23. Earthquake hazard curve for F2 Fault (Zare'e-orthogonal component)

Seismic Source Six: Tafresh Fault

A) Determination of Maximum Horizontal Acceleration:
PGA values per different magnitudes and distances of each segment of Tafresh Fault (seismic source 6) to the center of Borujerd are as shown in Fig 24 and 25.

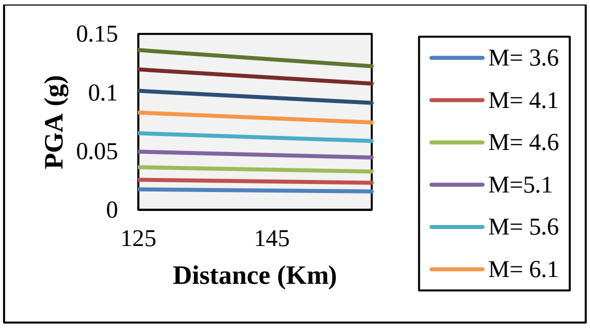

Fig 24. Attenuation estimation for Tafresh Fault (Zare'e-horizontal component)

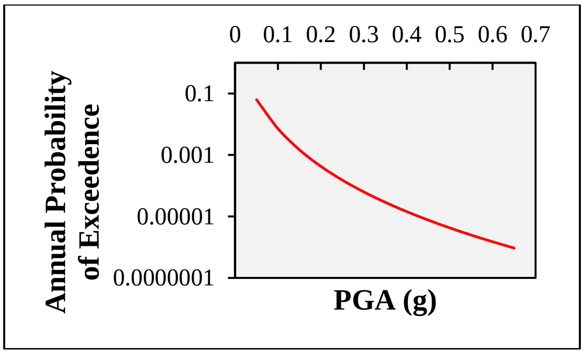

Fig 25. Earthquake hazard curve for Tafresh Fault (Zare'e-horizontal component)

B) Determination of Maximum Orthogonal Acceleration:
Fig 26 and 27 show the attenuation estimations of the orthogonal acceleration component according to relations proposed by Zare'e.

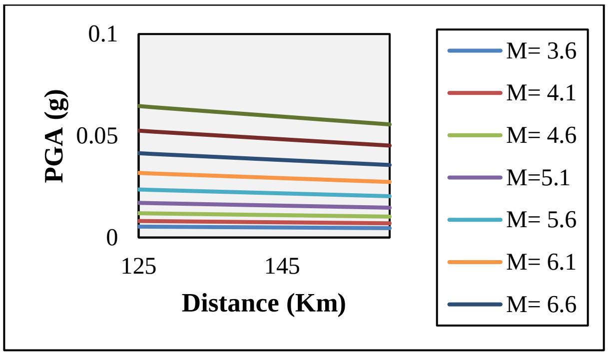

Fig 26. attenuation estimation for Tafresh Fault (Zare'e-orthogonal component)

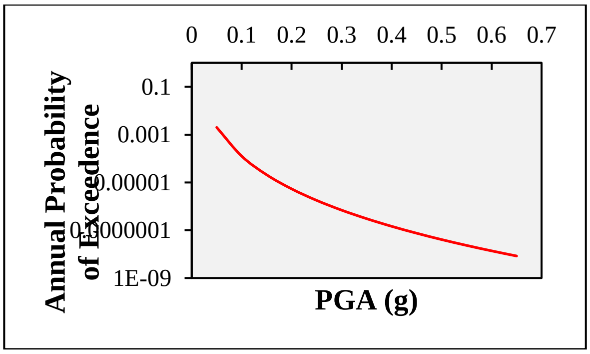

Fig 27. Earthquake hazard curve for Tafresh Fault (Zare'e-orthogonal component)

Seismic Source Seven: Main Zagros Reverse Fault (M.Z.R.F)

A) Determination of the Maximum Horizontal Acceleration:
PGA values per different magnitudes and distances of each segment of M.Z.R. Fault (seismic source 7) to the center of Borujerd are as displayed in Fig 28 and 29.

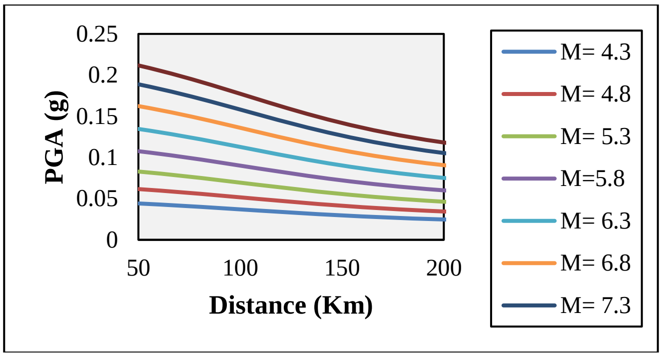

Fig 28. Attenuation estimation for M.Z.R. Fault (Zare'e-horizontal component)

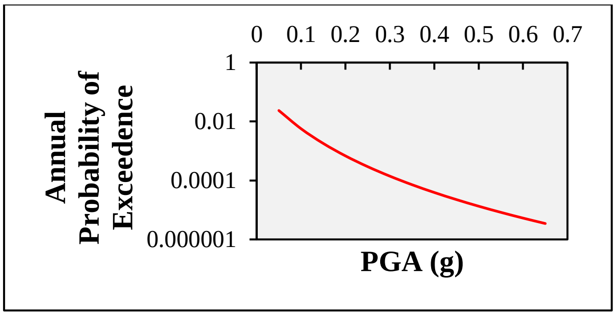

Fig 29. Earthquake hazard curve for M.Z.R. Fault (Zare'e-horizontal component)

B) Determination of Maximum Orthogonal Acceleration:
Fig 30 and 31 demonstrate the attenuation estimations for the orthogonal acceleration component according to the relations designed by Zare'e and Nowruzi.

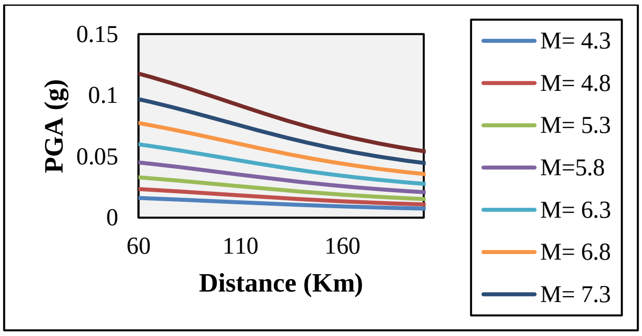

Fig 30. Attenuation estimation for M.Z.R. Fault (Zare'e-orthogonal component)

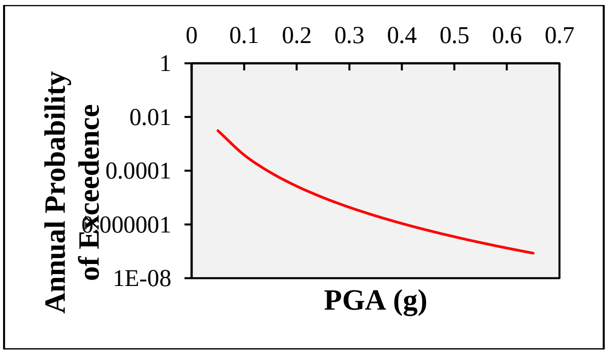

Fig 31. Earthquake hazard curve for M.Z.R. Fault (Zare'e-orthogonal component)

Seismic Source Eight: Dorud Fault

A) Determination of Maximum Horizontal Acceleration:
PGA values per different magnitudes and distances of each segment of Dorud Fault (seismic source 8) to the center of Borujerd are as illustrated in Fig 32 and 33.

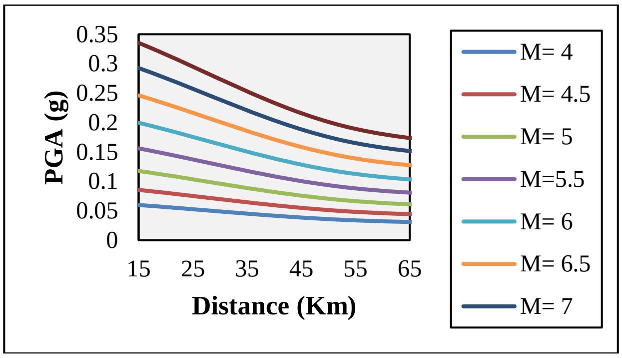

Fig 32. Attenuation estimation for Dorud Fault (Zare'e-horizontal component)

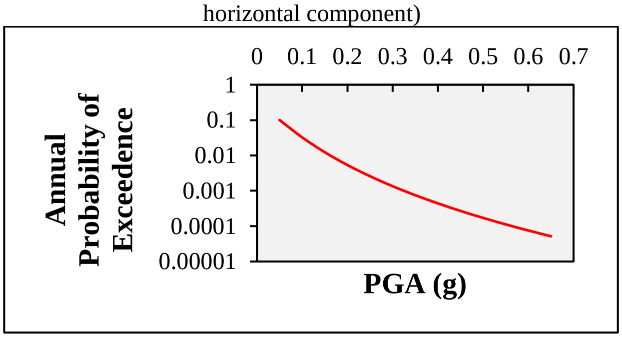

Fig 33. earthquake hazard curve for Dorud Fault (Zare'e-horizontal component)

B) B) Determination of Maximum Orthogonal Acceleration:
Fig 34 and 35 exhibit the attenuation estimations for the orthogonal acceleration component according to the relations offered by Zare'e.

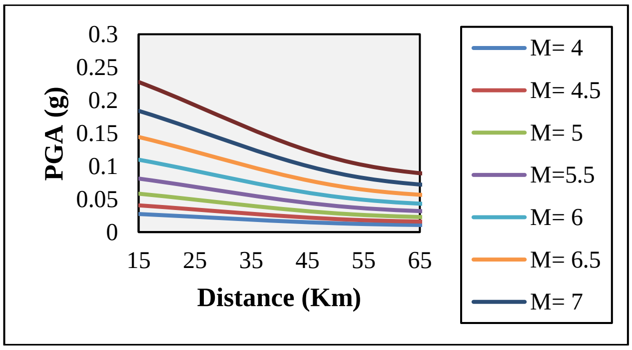

Fig 34. Attenuation estimation for Dorud Fault (Zare'e-orthogonal component)

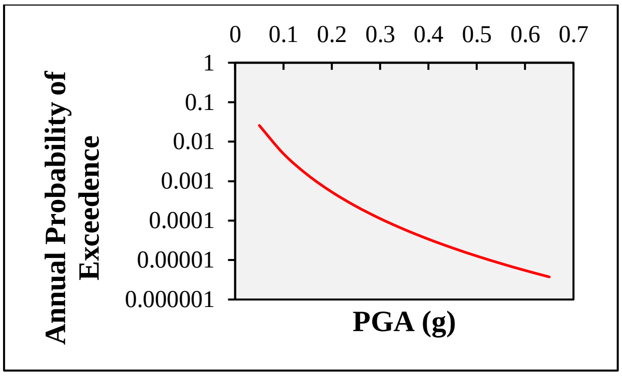

Fig 35. Earthquake hazard curve for Dorud Fault (Zare'e-orthogonal component)

Seismic Source Nine: Nahavand Fault

A) Determination of Maximum Horizontal Acceleration:
PGA values per different magnitudes and distances of each segment of Nahavand Fault (seismic source 9) to the center of Borujerd are as shown in Fig 36 and 37.

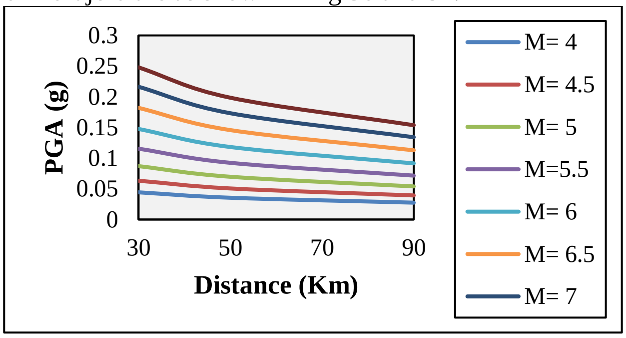

Fig 36. Attenuation estimation for Nahavand Fault (Zare'e-horizontal component)

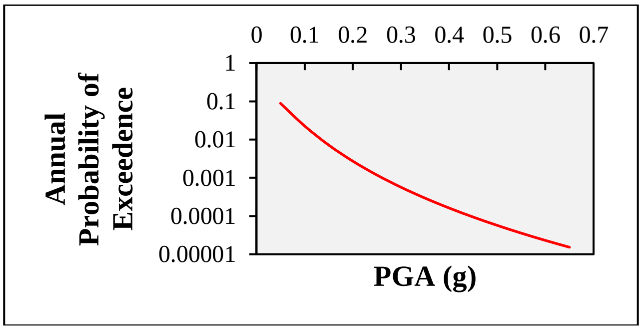

Fig 37. earthquake hazard curve for Nahavand Fault (Zare'e-horizontal component)

B) Determination of Maximum Orthogonal Acceleration:
Fig 38 and 39 display the attenuation estimations of the orthogonal acceleration component according to the relations offered by Zare'e.

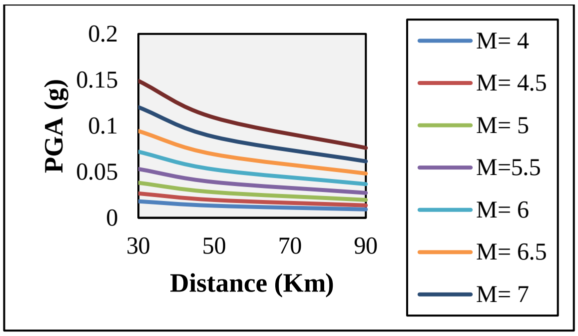

Fig 38. attenuation estimation for Nahavand Fault (Zare'e-orthogonal component)

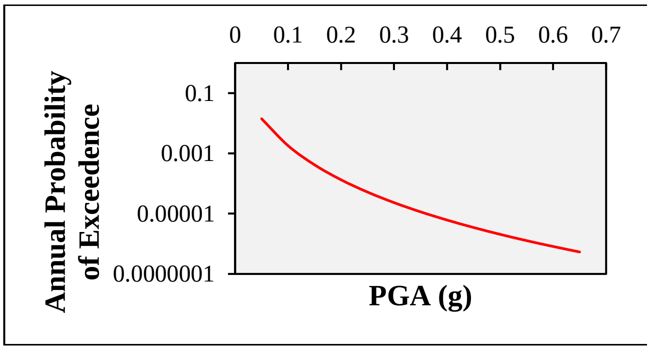

Fig 39. earthquake hazard curve for Nahavand Fault (Zare'e-orthogonal component)

Hazard Curve for the City of Borujerd

Combining the results obtained from the hazard curves pertaining to each of the selected seismic sources, the hazard curve of the city of Borujerd is as shown in Fig 40.

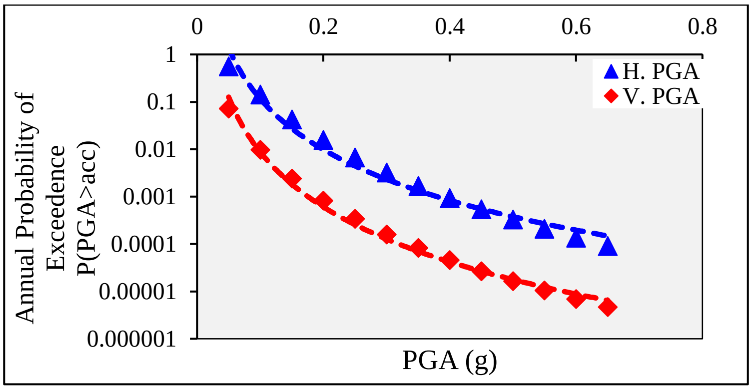

Fig 40. Hazard curve of the city of Borujerd

The combined hazard curve in the above figure has been obtained using power fit estimation and the estimated curve equations are as demonstrated beneath for horizontal and orthogonal states:

$$Hor: P = 3 \times 10^{-5} \times (PGA)^{-3.559} R^2 = 0.9775 \quad (11)$$

$$Ver: P = 1 \times 10^{-6} \times (PGA)^{-3.851} R^2 = 0.9919 \quad (12)$$

Substituting the values of the earthquake occurrence likelihood in the aforesaid equations, PGA values can be expressed as summarized in table 7.

Table 7. Maximum acceleration values for the various return periods

Occurrence likelihood (%)	In year	Return period	Design level	Horizontal acceleration (g)	Orthogonal acceleration (g)
10	100	950	MDE	0.37	0.16
10	50	475	DBE	0.30	0.14
50	100	145	OBE	0.22	0.10
50	50	73	-	0.18	0.08
10	1	10	-	0.10	0.05

As it is seen in Table 7, the largest DBE design level horizontal and orthogonal accelerations are 0.30g and 0.14g, respectively, and the largest OBE design level horizontal and orthogonal accelerations are 0.22g and 0.10g, respectively.

Conclusion

In terms of geotectonic, the study region is positioned in Zagros and Sanandaj-Sirjan structural zones that feature a relatively large seismic activity. The occurrence of many earthquakes in shallow depths with intermediate return periods signifies the existence of faults with rocky foundations in this region. Thus, the existence of the aerial magnetism data is of considerable importance for the identification of the slope and stretches of these types of faults. The dominant mechanism of the vibrations in the study region is of the strike-strip type with reverse indicator and/or of the reverse type with strike-slip indicator; the vibrations usually occur on the faults (of the thrust or reverse diagonal-slip type) along the two northwestern-southeastern and northern-southern trends. The most important seismic sources in the periphery of the region are Dorud, Nahavand, Sahneh, High Zagros, main Zagros thrust, Lahbari, and Zardkuh Faults. Considering the seismicity pattern of Zagros in the study region and the relative scattering of the earthquakes in the vicinity of the primary faults, it is suggested that most of the seismic sources should be linearly modeled. To study the earthquake hazard in Borujerd County, deterministic and probabilistic methods have been used with the summary of the studies and the most important obtained results being as explained underneath:

The investigation of the region's seismicity within a 200-kilometer radius shows that large earthquakes with magnitudes equal to Ms=7.4 have occurred with the faults being the primary cause of them. The statistical studies of the earthquakes are reflective of the idea that the earthquakes of this region are mostly with magnitudes in a range of Ms=4-5.5 and that they predominantly occur in shallow depths and stem from the earth crust. To study the seismicity and earthquake hazard within the 200-kilometer radius of the study region, deterministic and probabilistic methods were applied. In this study, the raw catalog available in such credible databases as ISC and USGS were utilized and the method designed by Gardner and Knopoff (1974) was utilized for associated earthquakes' declustering. The seismological parameters were completed using the method offered by Kiko and subsequently used as the basis of analyses. In the present study, updated attenuation relations by Zare'e were blended and used for performing deterministic and probabilistic analyses. Based on the obtained results, the maximum seismic power of the intended faults was in a range from 5.8 to 7.8 in the Richter scale on average. Additionally, the largest seismic power was found pertinent to the main Zagros fault (M=7.80, high Zagros fault (M=7.6), Kushk Nosrat Fault (M=7.5), Lahbari (M=7.5), F3 (M=7.4), Zardkuh (M=7.2) and Ardal (M=7.4). The largest horizontal accelerations obtained in the deterministic approach are 0.23g, 0.18g, and 0.17g correspondingly related to a high Zagros fault (H.Z.F), Nahavand Fault and Dorud Fault. Moreover, the largest orthogonal acceleration obtained in the deterministic approach is 0.11g, 0.09g and 0.08g respectively belonging to the high Zagros fault (H.Z.F), Nahavand Fault and Dorud Fault. Furthermore, in the probabilistic approach and DBE design level, the largest horizontal and orthogonal accelerations are 0.30g and 0.14g, respectively; the highest horizontal and orthogonal accelerations in the OBE design level were respectively found equal to 0.22g and 0.10g. In this research, mass changes were evaluated based on GRACE and GRACE-FO. Greenland is one of the most sensitive areas to mass loss of more than 0.2 m per year due to melting ice. Also, CSL is decreasing at an annual rate of 0.03m and has different decreasing rates from north to south and center (Bruneau et al., 2016; Van Baak et al., 2019; Kostianoy et al., 2019).

CSL was investigated with GRACE and GRACE-FO satellites. Significant results have been achieved by applying preprocessing steps to reach sea level. So the changes in CSL in the north and south are not the same. In the north of the CSL, the changes are twice as small as in the south and center of the CSL. A closer look requires measuring in-situ observations and other sensors. However, according to research, the temperature in the north of CS is much lower than the south and center (Bruneau et al., 2016; Van Baak et al., 2019; Kostianoy et al., 2019), which can be the main cause of the difference in CSL. Also, the depth of the CS in the north is less than in the south and center, which can be another effective factor. According to research, the flow of the Volga River is also a reduction that is the main feeder of CS (Seyedvalizadeh et al., 2020). Further research to predict CSL and TWS can also be done with artificial intelligence (Sorkhabi et al., 2022a; Sorkhabi et al., 2022b).

References

Aram, M. R. and Hasankhani, A., (2017), "simulation of the strong ground motions and offering attenuation relations for the construction site of Bushehr's atomic power plant based on the stochastic finite fault method", journal of nuclear sciences and techniques, 38(3): 58-72

Aryan V., Mehran and Pourkermani, Mohsen, (1997), "seismotectonic: tectonics quake", 1st ed., Alavi

Judaki, M.; Basereh, M.; Farzipour Sa'ein, A. and Safa'ei, H., (2013), "seismotectonic investigation and earthquake hazard analysis in the domain of Dorud County", 8th conference of Iran's association of geological engineering and environment, Ferdowsi University, Mashhad Branch

Rezapour, M., (2009), "analyzing the earthquake that occurred on 31st of March, 2006, in Silakhor in Lorestan Province", journal of Iran's geophysics, v.3, (1): 75-89

Zamani, A. and Agh-Atabai, M., (2008), "quantitative assessment of the spatial-temporal distribution of the aftershocks of the earthquake that occurred in 2006 in Darb Astaneh (Silakhor), in west of Iran", seasonal journal of geological sciences, (65): 70-79.

Authemayou, C., Chardon, D., Bellier, O., Malekzade, Z., Shabanian, E. and Abbassi, M.R., 2006. Late Cenozoic partitioning of oblique plate convergence in the Zagros fold-and-thrust belt (Iran). Tectonics, 25:1–21. doi:10.1029/2005TCOO1860.

Bayraktar, A., Hökelekli, E., Halifeoğlu, F.M ., Mosallam, A and Halil Karadeniz.2018. Vertical strong ground motion effects on seismic damage propagations of historical masonry rectangular minarets, Engineering Failure Analysis, Volume 91, September 2018, Pages 115-128.

Berberian, M., 1976 , Contribution to the Seismotectonics of Iran , Part II, Geol. Surv. Iran, 39 , p 518.

Berberian, M., 1995. Master blind thrust faults hidden under the Zagros folds: active basement tectonics and surface morphotectonics. Tectonophysics, 241:193–224.

Blanc, E. J.-P., Allen, M. B., Inger, S. and Hassani, H., 2003. Structural styles in the Zagros Simple Folded Zone, Iran. J. geol. Soc. Lond.,160, 401–412.

Forte, A.M., Cowgill, E., Bernardin, T., Kreylos, O. and Hamann, B., 2010. Late Cenozoic deformation of the

Kura fold-thrust belt, southern Greater Caucasus. G. S A. Bull., v. 122; no. 3/4; p. 465–486; doi: 10.1130/B26464.1.

Jackson, J. and McKenzie, D., 1984. Active tectonics of the Alpine–Himalayan Belt between western Turkey and Pakistan. Geophys. J. R. Astron. Soc., 77:185–264.

Jackson, J.,1992. Partitioning of strike-slip and convergent motion between Eurasia and Arabia in eastern Turkey and the Caucasus. J Geophys. Res. 97, 12:471-479.

Lü, Q., Chen, P., Kim, B., Zheng, J and Ji, J.2019. Probabilistic assessment of seismic stability of a rock slope by combining the simulation of stochastic ground motion with permanent displacement analysis, Engineering Geology, Volume 260.

Molnar, P. and Dayem, K.E., 2010. Major intracontinental strike-slip faults and contrasts in lithospheric strength. Geosphere; v. 6; no. 4; p. 444–467; doi: 10.1130/GES00519.1.

Sokolov , V and Wenzel, F . 2019. Areal exceedance of ground motion as a characteristic of multiple-site seismic hazard: Sensitivity analysis, Soil Dynamics and Earthquake Engineering, Volume 126.

Talebian, M. and Jackson, J., 2004. A reappraisal of earthquake focal mechanisms and active shortening in the Zagros mountains of Iran. Geophys. J. Int. 156:506–526.

Vaez Shoushtari, A., Bin Adnan, A and Mehdi Zare, M. 2018. Incorporating the local faults effects in development of seismic ground-motion hazard mapping for the Peninsular Malaysia region, Journal of Asian Earth Sciences, Volume 163, 1 September 2018, Pages 194-211.

Vernant, P., Nilforoushan, F., Hatzfeld, D., Abassi, M.R., Vigny, C., Masson, F,, Nankali, H., Martinod, J., Ashtiani, M., Bayer, R., Tavakoli, F. and Chéry, J., 2004. Present-day crustal deformation and plate kinematics in the Middle East constrained by GPS measurements in Iran and northern Oman. Geophys. J. Int., 157:381–398.

Wang, D and Gao, Y. 2019. A study on the selection of ground motion measures for seismic capacity assessments of urban building complexes in Weinan, International Journal of Disaster Risk Reduction, Available online 16 September 2019, 101333, In Press, Journal Pre-proof.

Xu,B., Wang, X., Pang, R and ZhouY, 2018. Influence of strong motion duration on the seismic performance of high CFRDs based on elastoplastic analysis, Soil Dynamics and Earthquake Engineering, Volume 114, November 2018, Pages 438-447.

Yuqiao, Q. I. N., T. A. N. G. Hua., D. E. N. G. Qin., Y. I. N. Xiaotao and W. A. N. G. Dongying. 2019. Regional seismic slope assessment improvements considering slope aspect and vertical ground motion, Engineering Geology, Volume 259.

Zamani, A., Hashemi, N., 2000 , A comparison between seismicity, topographic relief, and gravity anomalies of the Iranian Plateau , Tectonophysics, 327 , pp.25-36.

Zamani.A., Agh-Atabai.M., 2009 , Temporal characteristics of seismicity in the Alborz and Zagros regions of Iran, using a multifractal approach , Journal of Geodynamics , Vol 47, Issue 5, pp 271–279.